

Article

Photocatalytic Activity of TiO₂/AuNRs–SiO₂ Nanocomposites Applied to Building Materials

Alessandra Truppi ¹, Manuel Luna ² , Francesca Petronella ¹ , Aurelia Falcicchio ³,
Cinzia Giannini ³ , Roberto Comparelli ^{1,*} and Maria J. Mosquera ^{2,*} 

¹ CNR-IPCF, Istituto per i Processi Chimici e Fisici, U.O.S. Bari, c/o Dip. Chimica Via Orabona 4, 70126 Bari, Italy; a.truppi@ba.ipcf.cnr.it (A.T.); f.petronella@ba.ipcf.cnr.it (F.P.)

² TEP-243 Nanomaterials Group, Departamento de Química Física, Facultad de Ciencias, Campus Río San Pedro, Universidad de Cádiz, 11510 Puerto Real, Spain; manuel.luna@uca.es

³ CNR-IC, Istituto di Cristallografia, Consiglio Nazionale delle Ricerche, v. Amendola 122/O, 70126 Bari, Italy; aurelia.falcicchio@ic.cnr.it (A.F.); cinzia.giannini@ic.cnr.it (C.G.)

* Correspondence: roberto.comparelli@cnr.it (R.C.); mariajesus.mosquera@uca.es (M.J.M.); Tel.: +39-0805442027 (R.C.); +34-956016331 (M.J.M.)

Received: 4 July 2018; Accepted: 17 August 2018; Published: 22 August 2018



Abstract: In this work, the self-cleaning and photocatalytic properties of mesoporous TiO₂/AuNRs–SiO₂ composites (namely UCA–TiO₂Au) prepared by a simple and low-cost technique were investigated toward application in building materials. Mesoporous photocatalytic nanocomposites coating the surface of stone and other building materials are a very promising approach to address relevant questions connected with the increasing atmospheric pollution. We tested three types of preformed TiO₂/AuNRs nanostructures in order to evaluate the effect of AuNRs on the photocatalytic activity of resulting coatings deposited on the surface of a popular building limestone. The resulting nanocomposites provide crack-free surface coatings on limestone, effective adhesion, improve the stone mechanical properties and impart hydrophobic and self-cleaning properties. Photocatalytic characterization involved the degradation of a target compound (Methylene blue; MB) under direct exposure to simulated solar light using TiO₂ P25 Evonik (TiO₂ P25) as a reference material. Moreover, these coatings upon irradiation by simulated solar light were successfully employed for the photocatalytic oxidation of carbon soot. The experimental results revealed that UCA–TiO₂Au samples are the best performing coating in both MB bleaching and soot degradation.

Keywords: photocatalytic activity; self-cleaning; nanocomposites; silica matrix; gold modified titanium dioxide; building materials

1. Introduction

Nowadays, one of the most important issues in all the cities of the world is air pollution, which causes damage to structures and buildings, involving a global aesthetic, economic and ecological loss [1]. Since antiquity, stone has been one of the most often employed materials in the construction industry to create buildings. However, its surfaces can undergo deterioration over time due to several sources of damage, such as polluting gases and fine particulates, soluble and insoluble salts inside the porous matrix, acid rains that produce so-called “black crusts”, and many other human activities [2,3]. In addition, other deleterious processes may be: growth of organisms, bird droppings, fire damage, salt efflorescence, building defect, design features, external factors and stone characteristics. In recent years, the blackening of architectural surfaces is an important degradation process mostly for modern buildings, due to the need to not alter the aesthetic properties of their outdoor surfaces [2].

Titania-mediated photocatalysis is a very promising approach to address the increasingly crucial issues connected with environmental pollution [4,5]. Indeed, among the possible solutions, TiO₂ coating on building materials can significantly degrade a variety of organic and inorganic pollutants thanks to its unique photocatalytic properties, which contribute to its air-purifying and self-cleaning abilities [5–7].

Several self-cleaning/photocatalytic building materials have been available since the 1990s [6]. These self-cleaning coatings are advantageous thanks to the combination of the photocatalytic property and superhydrophilic character of TiO₂. Indeed, the photocatalytic reaction can promote the degradation of pollutants, while the wettability features remove definitively the broken-down deposits [5]. Several products such as cementitious materials, tiles and glass have been widely commercialized. TOTO Ltd., Tokyo, Japan, registered about 270 patents, producing white ceramic tiles for outdoor and indoor walls. Another important commercial product among the self-cleaning building materials is Neat Glass, produced by Cardinal Glass Industries. This material consists of a TiO₂ layer combined with a thin layer of silicon dioxide, which provide hydrophilicity and smoothness to the glass surface. Another system has been set up from Pilkington Group. Pilkington Active is a hydrophilic coating obtained with organic molecules and TiO₂ suitable for production of external glass [8].

In the literature, several studies have also demonstrated the high performances of TiO₂ coating employed for photooxidation of soot under illumination, despite of this oxidation process is rather slow [9,10]. Chin et al. reported a kinetic model for photocatalytic oxidation of soot to CO₂, which supposed two oxidation mechanisms: a single-step way and a multi-step way with a solid intermediate species [11,12].

The photoactivation process of a semiconductor takes place in the presence of light with suitable wavelength, promoting to generation of the electron-hole (e⁻h⁺) pair, which give rise to oxidative processes that potentially lead to remove polluting organic substances from water or air, by means of Reactive Oxygen Species (ROS) obtained from the reaction with oxygen molecules or water molecules [13]. TiO₂ has been deeply studied for decades and has been extensively used as reference material for many applications in the field of photocatalysis [14–16]. In spite of this, the pure TiO₂ can absorb only the UV region ($\lambda < 390$ nm), just a small fraction (4%) of the whole solar energy spectrum, because of its wide band gap, thus not allowing a deeper exploitation of natural sunlight for photocatalytic applications [4]. In addition, the efficiency of the photocatalytic process is affected by the competition between life-time of photo-generated electron-hole (e⁻h⁺) pairs and their recombination rate [17]. In the literature, many strategies have been developed to overcome these serious drawbacks.

The modified TiO₂ based photocatalysts are one of the most promising resolutions for these issues, offering the possibility to enhance air and health quality by removing environmental pollutants [18,19]. In particular, plasmonic nanostructures of noble metals in combination with semiconductors are attracting tremendous attention [20]. Notably, these hybrid photocatalysts are a brilliant strategy to improve the photocatalytic activity of TiO₂ due to the unique optical and electric properties of plasmonic metals [21,22]. Indeed, noble metals are expected to act like electrons traps, thus hindering the recombination of charge carriers and facilitating the transfer of holes on the TiO₂ surface. In particular, gold nanorods (AuNRs) have attracted a lot of interest due to their strong optical absorption in the visible range (Localized Surface Plasmon Resonance (LSPR)) [23]. However, it is well noted that the role played by gold nanoparticles (AuNPs) in the photoactivation mechanism is dependent on the impinging wavelength. Under UV irradiation, only TiO₂ is activated and photo-generated electrons are injected to noble metal NPs, inhibiting the charge recombination and finally increasing the photocatalytic activity. While, under visible-light irradiation TiO₂ cannot be photoexcited, thus light must be absorbed by plasmonic NPs. In addition, several possible photoactivation mechanisms of TiO₂/plasmonic NPs under visible-light irradiation have been recently suggested, i.e., charge and energy transfer [24]. Zhang et al. suggested three possible mechanisms: (i) plasmon resonance effect: under visible radiation, photoexcited metal NPs inject electrons into the conduction band of the semiconductor; (ii) near field effect: an electric field can be induced

by the plasmon resonance, promoting a plasmon resonance energy transfer (PRET) from metal to semiconductor. A rapid formation of e^-/h^+ pairs can be obtained thanks to an improvement of the electric field in a well-defined location of the TiO_2 due to the PRET; (iii) far field effect: an efficient scattering can be mediated by LSPR, which enhances the optical path of photons in TiO_2 facilitating the photogeneration of e^-/h^+ pairs [25].

Therefore, the unique combination of properties in $TiO_2/AuNRs$ makes it very appropriate for photocatalytic applications. Furthermore, the encapsulation of $TiO_2/AuNRs$ inside the mesoporous networks may be a powerful method for enhancing the photoactivity. Silica is usually chosen as matrix due to its capability to bind a range of several particles into its network and to improve the activity and selectivity of the photocatalyst. In particular, the encapsulation of TiO_2 into SiO_2 has always been considered an attractive methodology to obtain advanced materials, which are potentially used as heterogeneous catalysts and catalytic supports [26,27].

Photocatalytic TiO_2 nanoparticles can be incorporated in a mesoporous silica matrix in several ways, but the synthesis of TiO_2-SiO_2 nanocomposites by mixing the preformed TiO_2 NPs in a Si alkoxide sol represents an interesting method [1]. Recently, AuNPs were added to these nanocomposites [28] in order to promote absorption in the visible range. These NPs significantly improved the TiO_2 photoactivity under solar radiation.

The goal of the present work is to set up the synthesis of visible-light-active Au modified TiO_2-SiO_2 nanocomposites (namely UCA- TiO_2 Au), for potential application in building materials. In particular, in this work UCA- TiO_2 Au nanocomposite coating was prepared using a strategy previously reported [1,28]. In the present work, we took a step forward by employing anisotropic Au NRs in mesoporous TiO_2-SiO_2 composites to enhance the visible-light photocatalytic performance. Specifically we have synthesized crack-free mesoporous xerogels by dispersion of preformed $TiO_2/AuNRs$ hybrid nanoparticles in a mesoporous silica matrix in the presence of *n*-octylamine (non-ionic surfactant) [29]. The several roles of *n*-octylamine are well-known. It can act: (1) to prevent the unwanted aggregation of Titania particles in the starting sol; (2) as a basic catalyst of the sol-gel transition; and (3) to obtain mesoporous silica network, by an inverse micelle mechanism, thus preventing unwanted cracking of silica xerogels [30].

We have investigated synthesis and characterization of UCA- TiO_2 AuNRs nanocomposite coating in three different types of preformed $TiO_2/AuNRs$ to observe the relative effect on the photocatalytic performance of the stone (namely UCA- TiO_2 Au 250 °C, UCA- TiO_2 Au 450 °C and UCA- TiO_2 Au 650 °C). In particular, we applied the synthesized materials on a limestone widely used for construction of modern and ancient buildings and evaluated the performance of the coatings, such as photocatalytic properties, adhesion on the stone surface, hydrophobic properties and aesthetic characteristic. Furthermore, we investigated the structures of these materials using several techniques including TEM and nitrogen physisorption. Photocatalytic experiments were performed under simulated solar light in order to test the degradation of a target compound (Methylene Blue) deposited on stone, using UCA- TiO_2 P25 nanocomposite as a reference material. Moreover, these coatings upon simulated solar irradiation were successfully employed for the photocatalytic oxidation of soot. The obtained results highlight a strong enhancement in the photocatalytic performance of UCA- TiO_2 Au nanocomposite compared to pristine UCA- TiO_2 and UCA- TiO_2 P25 nanocomposites, arising from the presence of Au NRs. Finally, these results point out the possibility to shift the photocatalytic performance of mesoporous UCA- TiO_2 Au nanocomposites in the visible range and their feasibility for several environmental applications.

2. Materials and Methods

2.1. Materials

All chemicals were used as received without further purification. TES40 WN (ethoxysilane providing approximately 41% of silica upon complete hydrolysis) were purchased from Wacker Chemie AG,

Munich, Germany. *N*-octylamine (non-ionic surfactant), Titanyl sulfate (TiOSO_4 , 29% TiO_2 , 17% H_2SO_4), ammonium bicarbonate (NH_4HCO_3 , 99%), Methylene Blue (3,7-bis(Dimethylamino)-phenazathionium chloride, MB) and all solvents were purchased from Aldrich Chemical reagent (Darmstadt, Germany). All solvents used were of analytical grade. TiO_2 P25 Evonik (TiO_2 P25) was selected as commercial standard material. The carbon black Printex-U, delivered by Evonik, was used as model component for soot. MilliQ water was employed for preparation of all aqueous solutions.

2.2. Synthesis of Xerogels

2.2.1. Preformed TiO_2 /AuNRs

The synthesis of TiO_2 /AuNRs was performed by following a conventional co-precipitation technique [31]. AuNRs samples (aspect ratio 3.5 ± 0.5 ; longitudinal plasmon band at 780 nm) were synthesized by seed-mediated synthetic route [32] (Figure S1), and then dispersed in the aqueous solution of TiOSO_4 (1% *w/w* compared to TiO_2). Such a solution was hydrolyzed by drop-wise addition of NH_4HCO_3 under vigorous stirring, thus promoting the nucleation and precipitation of a pink slurry. Such paste was repeatedly washed by subsequent cycle of dispersion in water and centrifugation. The precipitate was dried in an oven overnight, milled and calcined at 250–450–650 °C for 2 h in a muffle in ambient atmosphere. Additionally, the counterpart TiO_2 materials without AuNRs were prepared. A detailed characterization of the obtained catalysts is reported as supplementary material.

2.2.2. Mesoporous Coating

Composite coatings were prepared by dispersion of preformed TiO_2 /AuNRs hybrid nanocatalyst in a silica oligomer (TES40) in the presence of a nonionic surfactant (*n*-octylamine). Syntheses were carried out as follows: TES40 was mixed with TiO_2 /Au and TiO_2 particles previously prepared (1% *w/v* compared to TES40; i.e., AuNRs loading in the resulting nanocomposite is estimated to be 0.01% *w/v*) in the presence of *n*-octylamine and water under high-power ultrasonic agitation (2.5 W cm^{-3}) for 10 min using a Sonopuls HD3200 ultrasonic homogenizer from Bandelin, Berlin, Germany. The proportion of *n*-octylamine and water to TES40 were 0.36% and 0.83% (*v/v*), respectively. Moreover, the water added to the sol is responsible for improving the hydrolysis of the silica precursor during all the sol-gel transition and for promoting the formation of condensed particles in presence of the *n*-octylamine. The obtained sols were designated as UCA- TiO_2 /Au XXX °C (containing TiO_2 /Au particles) and UCA- TiO_2 XXX °C (containing TiO_2 particles); XXX refers to the particle calcination temperature (250–450–650 °C). For comparative purposes, a TiO_2 /SiO₂ sol containing P25 particles and a sol without TiO_2 nanoparticles were prepared according to the same synthesis (namely UCA- TiO_2 P25 and UCA, respectively). A rough estimation of the material cost at a lab-scale is 170 €/L where 1 L of material is enough to coat a surface of 1.5 m².

2.3. Sol-Gel Characterization

Successively after the synthesis of the sols, their rheological properties were studied using a concentric cylinder viscosimeter (model DV-II+ with UL/Y adapter) from Brookfield. Experiments were carried out at a constant temperature of 25 °C maintained by recirculated water from a thermostatic bath. The viscosity was measured as the slope of the shear rate vs. shear stress curve, with the linear regression coefficient of above 0.99. Coatings of the materials under study were obtained by deposition of 3 mL of sol on plastic Petri dishes with a diameter of 85 mm. Dishes were covered and maintained at laboratory conditions (relative humidity of 60% and temperature of 20 °C). Gel transition and spontaneous drying took place giving rise xerogels, which were characterized after reaching constant weight. The pore volume, pore size distribution, and BET (Brunauer–Emmett–Teller) surface area of the coatings was characterized by Nitrogen Physisorption (Autosorb IQ from Quantachrome, Boynton Beach, FL, USA). The adsorption data were analyzed using a hybrid Non-Local Density Functional Theory (NLDFT) approach [33], which allows quantification of both micro- and mesopores

in order to obtain the pore size distribution of materials containing pores of different geometry. Transmission electron microscopy (TEM) analysis was performed by a JEOL 2010F TEM/STEM microscope (JEOL Ltd., Musahino, Japan), operating at 200 kV with 0.19 nm spatial resolution in high resolution transmission electron microscopy (HRTEM) mode. The TEM samples were prepared by casting a drop of catalyst suspension in water onto a carbon coated TEM grid. The chemical bonds in the coatings under study were analyzed by Fourier Transform Infrared Spectrophotometry (FTIR). The spectra were recorded in powder using a FTIR-8400S from Shimadzu (Shimadzu Corporation, Kyoto, Japan; 4 cm^{-1} resolution) in the region from 4000 to 700 cm^{-1} . Experiments were carried out in attenuated total reflection mode (ATR). X-ray Powder Diffraction (XPD) patterns were collected by a RIGAKU model RINT2500 diffractometer (Rigaku Corporation, Tokyo, Japan), with rotating anode (50 kV, 200 mA), silicon strip D/teX Ultra detector, Johansson Ge (111) asymmetric monochromator ($\lambda = 1.54056\text{ \AA}$). The measurements were carried out in transmission geometry by inserting the powders into 0.5 mm Lindemann capillaries. UV-Vis/DR spectra were recorded using UV-Vis diffuse reflectance spectrophotometer (Shimadzu UV-2600, Shimadzu Corporation, Kyoto, Japan), equipped with an integrating sphere (ISR-2600, Shimadzu Corporation, Kyoto, Japan), using BaSO_4 as reference. The band-gap energies were evaluated from the diffuse reflectance data, by using the Kubelka–Munk function, $F(R) = (1 - R^2)/2R$ and plotting of the Tauc plot, $(F(R)h\nu)^{1/2}$ vs. $h\nu$ [34,35].

2.4. Application on Stone and Characterization

The stone selected for evaluating the performance of UCA– TiO_2 –Au coatings is a fossiliferous limestone (calcite 98.5%, α -quartz 1.5%) [29], a natural product that has excellent technical and aesthetic characteristics. Its technical properties, its resistance and its elegant appearance has led to the use of this material for many centuries in the construction of a rich monumental heritage made up of official buildings, cathedrals, etc. Today, it is used in modern architecture to create elegant designs and architectural spaces, it is functional and may be considered aesthetically luxurious. It is a very hard and compact limestone the base color of which is white. The characteristics of this product make it especially suitable for placement in cladding of walls, both indoors and outdoors, facades and floors.

All the experiments were carried out using stone samples sizing $5 \times 5 \times 2\text{ cm}^3$ (l, d, h). The obtained sols were applied by spraying onto the surfaces of the stone samples until saturation, in 3 periods of 5 s. Moreover, the excess of sol was removed directly from the stone surface by air spraying. Next, the treated stones were dried at room temperature until reaching constant weight. Successively, we calculated the corresponding dry matter of products and characterized the samples by the procedures described below. In order to evaluate the adherence of the coating to the stone surface, the weight loss of stone was determined by performing a peeling test using Scotch Magic tape (3 M) [36]. The mechanical properties of treated stone were evaluated by using the Vickers hardness test method, also referred to as a microhardness test method [37]. Hardness is defined as the resistance to indentation, and it is determined by measuring the permanent depth of the indentation. In particular, the Vickers method is based on an indentation hardness test, using a calibrated machine to force a square-based pyramidal diamond indenter (RB2/Centaur DA 200 Durometer, Metrol Centaur s.l., Bilbao, Spain), under a pre-determined force ($30\text{ kg} \times 15\text{ s}$), into the surface of the material under test. The diagonals of the resulting impression are measured after removal of the load by a stereoscopic microscope (Nikon SMZ800, Nikon Corporation, Tokyo, Japan) and converted to a hardness value.

In order to evaluate the hydrophobic properties of the UCA– TiO_2 –Au coatings, contact angles of the stone surfaces were determined using a commercial video-based software-controlled contact angle analyzer, model OCA 15plus, from Dataphysics Instruments. We also investigated the changes in water absorption after treatments by measuring the water absorption by capillarity, according to UNI-EN 15801:2010 [38]. In addition, it was evaluated the possible change in stone color induced by the treatments with these mesoporous materials [39]. This disadvantageous effect was evaluated by a solid reflection spectrophotometer, Colorflex model, from Hunterlab, under the following conditions:

illuminant D65 and observer 10°. In particular, the color variations were measured by the total color difference parameter using CIE $L^*a^*b^*$ color space ($\Delta E^* = (\Delta L^2 + \Delta a^2 + \Delta b^2)^{1/2}$) [40].

2.5. Photocatalysis Experiments

Self-cleaning properties of the materials under study were evaluated by depositing a certain aliquot of Methylene Blue solution on the surface of stone specimens. First, 0.5 mL of a solution of 1 M Methylene blue in ethanol was deposited on the treated stone samples and their untreated counterparts. Next, the stone samples were irradiated with simulated solar light in a solar degradation chamber, (Solarbox 3000eRH from CO.FO.ME.GRA., Milano, Italy), equipped with a 2500 W xenon arc lamp and an outdoor UV filter, monitoring the temperature, humidity and irradiance (in 300–800 nm range) at the conditions employed were 300 W/m² of irradiance, 60 °C of temperature, 50% of humidity. We used the previously described solid reflection spectrophotometer to measure the reflectance spectra of surface samples. We reported the photocatalytic activity of each materials under study by using the absorbance variation in function of irradiation time according to a methodology based on the Kubelka–Munk theory proposed to study this type of dye degradation [28]. Furthermore, the photocatalytic oxidation of soot under simulated solar light irradiation was evaluated by a test adapted from the literature [41]. The carbon black Printex-U was used as model component for soot. A dispersion of 0.8 mg carbon black in 10 mL water was made and 650 µL were applied on each stone sample, resulting in a soot layer of 2 µg cm⁻², according to [41]. Next, the stone samples were irradiated in the solar degradation chamber working at 500 W/m², 70 °C, 60% humidity. The decoloration of the soot layer was monitored using the same methodology for MB degradation but employing the absorbance value at 600 nm due to the absence of maxima in the soot spectra.

3. Results and Discussion

3.1. TiO₂/AuNRs Characterization

Figure S2 reports the Transmission Electron Microscopy (TEM) images of TiO₂/AuNRs photocatalysts for different synthesis conditions, which confirm that AuNPs are mostly embedded in submicrometric aggregates composed of TiO₂NPs. A previous comprehensive characterization of these materials shows that, in spite of the drastic thermal treatment, in TiO₂/AuNRs nanocomposite, AuNRs mainly retain their shape and the size up to 450 °C. On the contrary, at higher calcination temperatures, the AuNRs undergo reshaping leading to spheres and ellipsoids. In particular, diffuse reflectance spectra (DRS) of TiO₂/Au NRs nanocomposites show a blue-shift and a broadening of longitudinal plasmon band absorption as a function of calcination temperature, as reported in Figure S3.

3.2. Sol-Gel Characterization

UCA–TiO₂Au nanocomposites are synthesized by a one-step, simple and low-cost technique, mixing ethoxysilane oligomers and TiO₂/AuNRs in presence of non-ionic surfactant (*n*-octylamine). In particular, we proposed TiO₂/AuNRs nanocomposite such as innovative visible-light active hybrid nanocatalyst to be incorporated in a mesoporous material, which was synthesized by a conventional co-precipitation technique and calcined at different temperatures (250–450–650 °C). The prepared sols had low viscosities (Table 1) and they should be able to penetrate deeper into the stone and should make easier the use of an aerosol generator to apply the product in situ [1,42]. In a previous study, Pinho et al. determined the viscosity for one of the most popular commercial stone consolidants, Tegovakon V100 from Evonik; the viscosity of this solvent-free product was 5.25 mPa s at 25 °C [43]. Therefore, we think that these obtained sols, with lower viscosities, must assure an adequate penetration into the stone pore structure, in a way similar to that of the commercial sols. Comparing the viscosities, it is observed that the values for the sols containing our TiO₂ particles are lower than the corresponding for the sol containing P25. This behavior can be attributed to the different nature of TiO₂ particles, specifically their different sizes. The lower size of P25 (25 nm) produces an increase

in the viscosity due to the small particles presenting higher interparticle interactions, which in turn produce bigger particle clusters in the sol [44].

Table 1. Viscosity values of sols at 25 °C and band gaps and textural for the mesoporous composites obtained from the sols.

Product	Viscosity (mPa·s)	Band Gap $\sim 10^{-2}$	Surface Area (m ² /g) ~ 1	Pore Volume (cm ³ /g) $\sim 5 \cdot 10^{-2}$	Pore Size (nm) $\sim 10^{-1}$
UCA	4.8 ± 0.1	–	654	0.42	1.3
UCA–TiO ₂ P25	6.1 ± 0.1	3.52	540	0.46	1.3
UCA–TiO ₂ 250 °C	4.3 ± 0.1	3.35	614	0.43	1.3
UCA–TiO ₂ 450 °C	4.4 ± 0.1	3.36	257	0.33	3.5
UCA–TiO ₂ 650 °C	4.7 ± 0.1	3.34	615	0.42	1.3
UCA–TiO ₂ Au 250 °C	4.9 ± 0.1	3.29	635	0.34	1.3
UCA–TiO ₂ Au 450 °C	5.0 ± 0.1	3.24	610	0.50	1.3
UCA–TiO ₂ Au 650 °C	4.8 ± 0.1	3.22	613	0.40	1.3

The sol-gel transition occurred in a maximum time of 48 h for all sols and, after two weeks of drying, we evaluated the morphological and optical properties of the obtained homogeneous composite gel. Figure 1 presents representative images from HRTEM taken at two different magnification scales. A silica matrix composed of an aggregation of amorphous silica particles is clearly observed for the xerogels, with sizes ranging from 20–25 nm in UCA and slightly smaller silica particles for UCA–TiO₂Au 450 °C, confirming the silica particle formation by *n*-octylamine action [30]. This reduction in the silica particle size has been previously reported and it is explained as the presence of preformed particles promoting silica nucleation [28]. In addition, the TiO₂ and TiO₂/AuNRs are embedded in the silica matrix in the form of aggregates of 200–300 nm, producing the TiO₂/SiO₂ nanomaterial. This confirms that the TiO₂ particles in the sols are bigger than the P25. These particles are distinguishable from the SiO₂ matrix due to their different contrast (one of them is easily observed in the center of Figure 1D). The nature of these particles is confirmed at higher magnification where the lattice planes corresponding to anatase (Figure 1E) and gold (Figure 1F) were observed. However, the observation of these crystalline structures was difficult due to the overlapping of the different TiO₂ crystallites composed the TiO₂/AuNRs composite and the SiO₂ matrix covering them; therefore, only the planes of TiO₂ crystallites and AuNRs with the proper distribution and orientation could be observed.

In addition, Figure S4 shows the XPD patterns collected on the UCA–TiO₂ (upper row) and UCA–TiO₂-Au (lower row) compounds. The largest contribution to the patterns comes from the UCA component, which was subtracted from the original data in Figure S4a,c to enhance the contribution of the TiO₂ nanocrystals and AuNRs. The as-subtracted patterns are displayed in Figure S4b,d and reveal few diffraction peaks which have been indexed as the reflections of TiO₂ anatase crystal structure (red markers) [45]. The contribution of the AuNRs (blue markers) was below the detection level.

Figure 2 shows the obtained FTIR spectra of all nanomaterials under study in this work. All the materials present several peaks typical of SiO₂, the bands located at 800 and 1080 cm⁻¹ are attributed to Si–O–Si bending; the band at 960 cm⁻¹ is attributed to Si–OH stretching and the broad band in the 3250–3750 cm⁻¹ range is attributed to Si–OH groups and absorbed molecular water on surface of materials. Only for SiO₂–TiO₂/Au nanocomposites, the Si–O–Si peaks are slightly shifted at higher wavenumbers. This shift in silica bands has been previously observed comparing the FTIR spectra of sols and dry xerogels [29], thus, the sol-gel reaction was more advanced for SiO₂–TiO₂/Au materials. In addition, other bands associated with no hydrolyzed ethoxy groups were also observed, including the characteristic C–H stretching bands at 2800–2900 cm⁻¹. These bands were especially intense in UCA–TiO₂ 450 °C, in addition another band related with ethoxy groups was observed for this material, CH₃ rocking at 1150 cm⁻¹ and also small bands assigned to *n*-octylamine. Contrary to the other xerogels, which were rigid and vitreous, UCA–TiO₂ 450 °C was more flexible and rubberlike.

These properties and the signals observed in the FTIR spectrum indicate that the sol-gel transition was not completed for UCA-TiO₂ 450 °C and it remained as a wet gel.

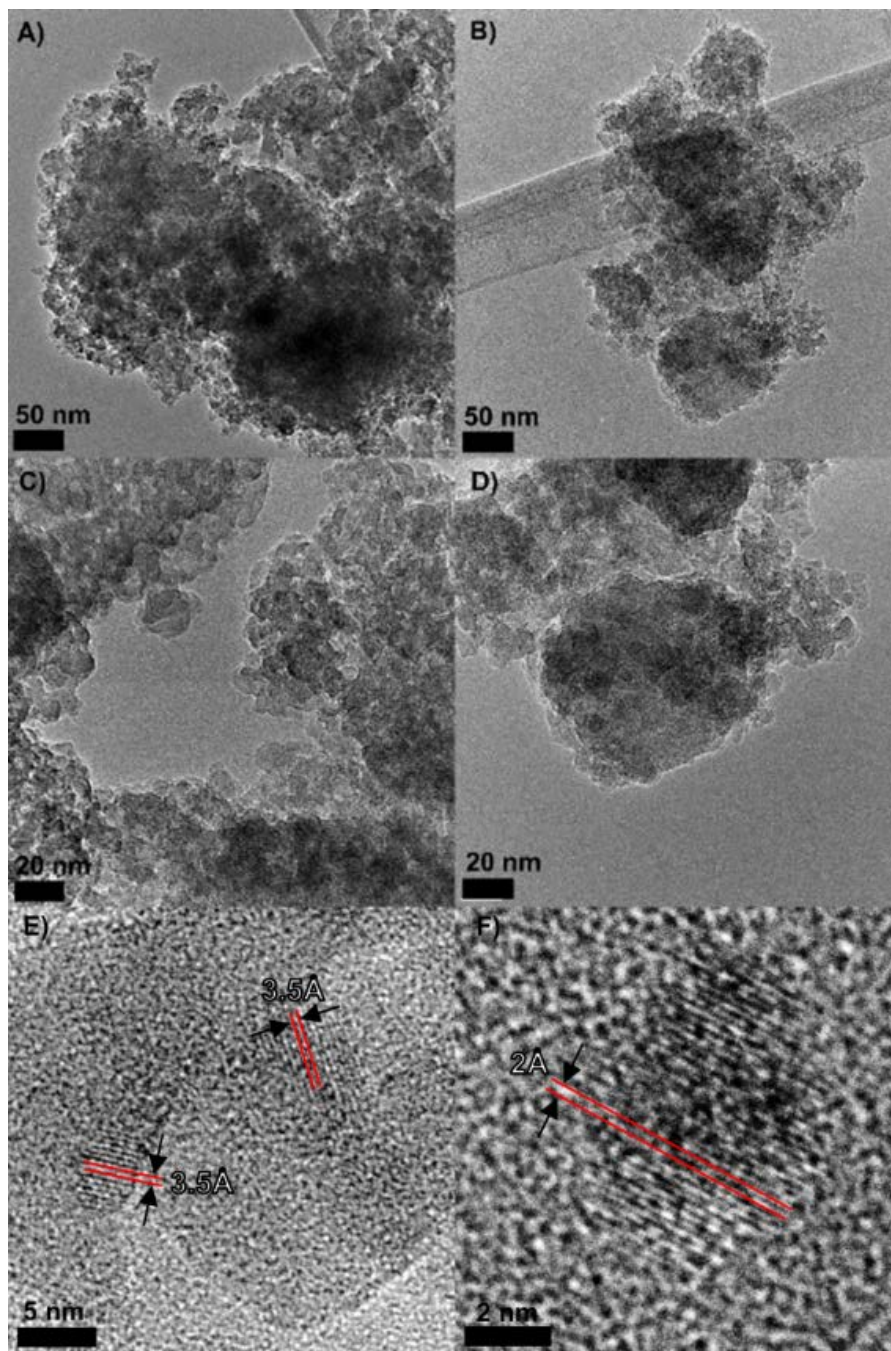


Figure 1. Representative high-resolution transmission electron microscopy (HRTEM) images obtained for the photocatalysts UCA (A,C), UCA-TiO₂Au 450 °C (B,D), interplanar spacing of TiO₂ (E) and Au (F).

In order to confirm the presence of AuNRs in the xerogels, we studied their optical behavior using the diffuse reflectance UV-Vis spectroscopy (Figure 3). We can observe that all the photocatalysts show absorption in the UV range (up to 400 nm). It is important to underline the fact that the major component of the UCA nanocomposites (SiO₂) does not absorb in the range of 200–800 nm. Furthermore, the UCA-TiO₂ photocatalysts do not show absorption in the visible range, attributed to

the fact that the TiO_2 nanoparticles in a mesoporous material does not change their optical behavior, whereas a marked modification of absorption properties for UCA- TiO_2/Au NRs compounds was observed. In particular, they showed a significant absorption in the visible region (400–700 nm). Specifically, the absorption spectrum of UCA- TiO_2/Au is characterized by two maxima for sample treated at 250–450 °C, characteristic of AuNRs. The first one is located around 530 nm (transversal excitation) and the other maximum appears at a longer wavelength (longitudinal excitation) [46]. This indicates that AuNRs are present in our $\text{TiO}_2/\text{SiO}_2$ xerogels and their shape was not altered during the synthesis due to the encapsulation inside the TiO_2 . On the other hand, the sample containing the TiO_2/Au calcined at higher temperature (650 °C) shows only one maximum centered at 680 nm (Figure S2) because AuNPs became spherical. It is well-known that the AuNRs at high temperature gradually shortened and ended at a certain aspect ratio until a spherical shape dependent on the annealing temperature [47,48]. Moreover, the values of energy gap (E_g) of these samples were obtained from the spectra illustrated in Figure 3 and reported in Table 1, by plotting $(F(R)hv)^{1/2}$ versus hv , according to the method proposed by Tandom [35]. The UCA- TiO_2/Au xerogels exhibit values of E_g in the range of 3.22 up to 3.29 eV, slightly lower than the corresponding ones for UCA- TiO_2 , as an effect of the presence of AuNRs.

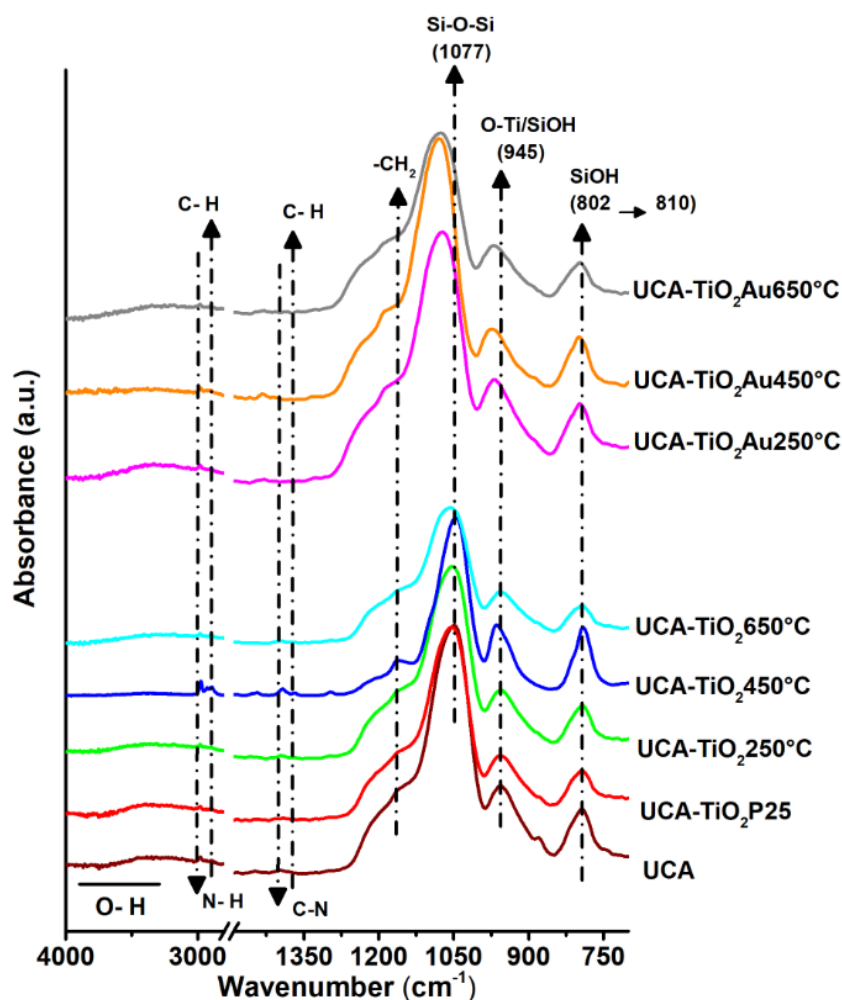


Figure 2. FTIR spectra of the synthesized UCA- TiO_2 nanocomposites under study.

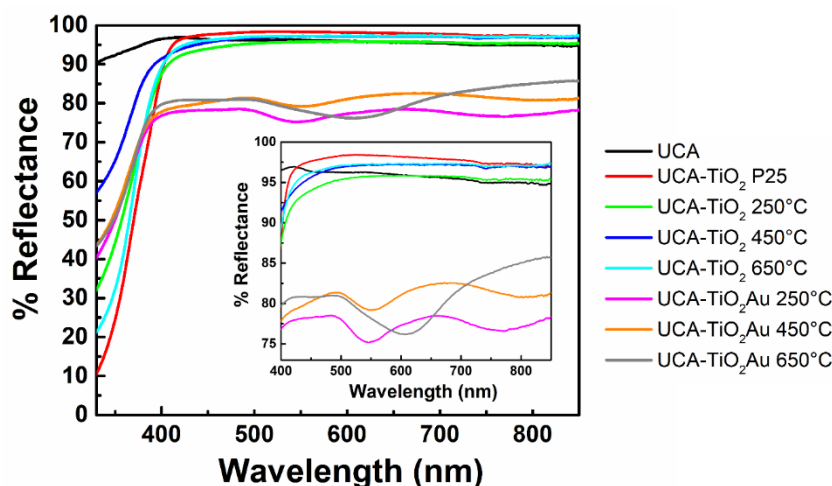


Figure 3. Diffuse reflectance spectra UV-Vis of UCA-TiO₂ and UCA-TiO₂Au nanocomposites powders under study. In the inset is reported the detail of visible range.

Successively, nitrogen physisorption tests were carried out in order to evaluate the texture of these composites. In Figure 4 are reported the adsorption–desorption isotherms and NLDFT pore size distributions obtained from the isotherm desorption branches for the materials under study. In more depth, the obtained textural results are shown in Table 1. All of the samples present a Type IV isotherm with a H2 hysteresis loop [49], as expected for a material with mesoporous structure. (Figure 4C,D). These isotherm profiles are characteristic of some types of silica materials that present a poor pore connectivity due to the presence of ink-bottle shape pores [50]. Pinho et al. have previously obtained similar morphologies, consisting of a dispersion of TiO₂ NPs inside a regular matrix of a uniform silica spheres [29,51]. Therefore, these isotherms indicate that all our materials are composed of a network of silica spheres due to the *n*-octylamine role and the TiO₂ particles are integrated within this network, as observed in TEM characterization. Most materials showed hysteresis H2(b) but UCA and UCA-TiO₂Au 250 °C have hysteresis H2(a); this change is due to these materials presenting a lower amount of big pores that promote the nitrogen cavitation or percolation during the test. In general, the materials containing TiO₂ have larger pores, due to an increase in the interparticle size produced by the presence of TiO₂ particles in the structure. Except for UCA-TiO₂ 450 °C, all the samples show adsorption at low pressure, which indicates that these materials have micropores. The absence of microporosity in UCA-TiO₂ 450 °C material can be related with the fact that it remains as a wet gel, the non-reacted silica precursor can fill these small pores preventing the nitrogen adsorption in them. All materials have similar surface areas and pore volumes, in particular, the UCA-TiO₂Au 450 °C material presents the pore volume higher than other samples and UCA-TiO₂Au 250 °C and UCA-TiO₂ 450 °C present lower values due to their differences previously described. Since the degradation processes studied in this work are surface phenomena the textural parameters are key factors for promoting the contact between the TiO₂ and the involved molecules [52–55]. A high surface area promotes the degradation processes [54,56–58] and the pore volume allows the molecule diffusion to activate photocatalyst sites through the pore structure [28,53,59,60].

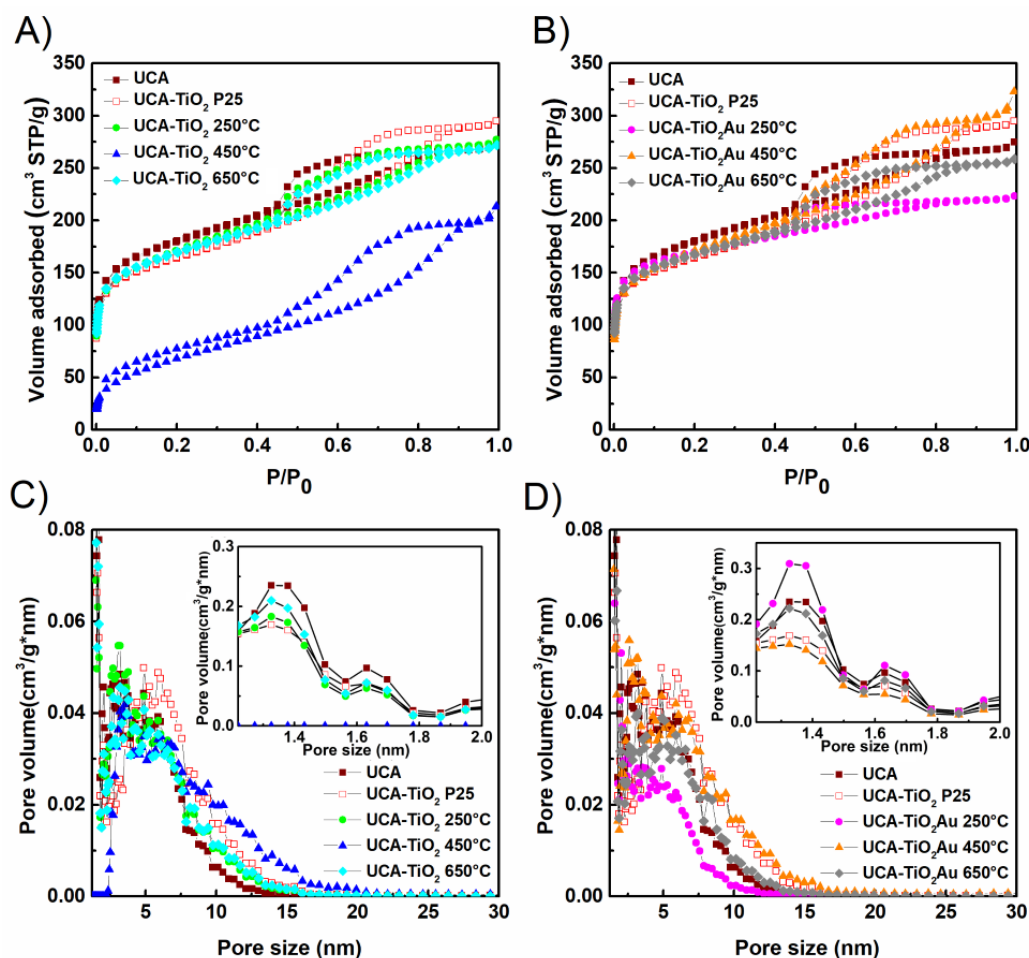


Figure 4. Nitrogen adsorption–desorption isotherms for the nanocomposite coatings under study: (A) UCA–TiO₂ series, (B) UCA–TiO₂Au series. NLDFT pore size distribution are shown in (C,D), respectively.

3.3. Application on Stone and Characterization

The new photocatalysts were sprayed as sols, under laboratory conditions, onto a building limestone in order to investigate its photocatalytic properties, its penetration depth, adhesion to the stone, and mechanical properties. We also investigated the effectiveness of UCA and UCA–TiO₂ P25 as comparison materials, which are composed of only silica and silica–TiO₂P25 respectively. Dry matter of the treatments is reported in Table 2. Some differences were observed between several samples due to the heterogeneity of the limestone samples, in particular the UCA sol produces the lowest dry matter among the sols applied, but any trend is not observed. Among the practical limitations of these photocatalytic coatings, the color changes of the treated stones is the most important issue [39]. The changes in the color (reported as ΔE^*) of the limestone induced by the coatings were measured and the obtained results are reported in Table 2. It was observed that all materials show a total color difference value (ΔE^*) close to the threshold value ($\Delta E^* \leq 5$), which is commonly used for the most restrictive applications such as ancient building restoration [61]. In particular, this parameter is critical for UCA–TiO₂Au sols due to the fact that their color is not white (the substrate color), but they produce color variations slightly higher than UCA–TiO₂ treatments (Figure S5). Indeed, TiO₂ is widely used as a white pigment producing a visible whitening effect on stone samples, while Au NRs contributes for the generation of colored nanocomposites. From these results, we conclude that our application method contributes to minimizing the color change of stone surfaces to suitable values, due to three important expedients: (i) by dispersing nanoparticles, these coatings also reduce the hiding power

of TiO₂ and Au and minimize the possibilities of significant color change; (ii) using a relatively low load of TiO₂/Au NRs (1% *w/v*); (iii) removing the excess of sol on the stone surface directly after its application.

Table 2. Properties of the treated stone specimens and the untreated counterparts.

Sample	Dry Matter (% <i>w/w</i>)	ΔE^* Color	Material Removed by Peeling (mg)	Contact Angles (CA)	Contact Angles after Irradiation
untreated	–	–	1.7 ± 0.3	–	–
UCA	0.45 ± 0.05	3.0 ± 0.1	0.2 ± 0.1	77 ± 5	50 ± 2
UCA–TiO ₂ P25	0.53 ± 0.02	4.0 ± 0.6	0.2 ± 0.1	82 ± 4	57 ± 3
UCA–TiO ₂ 250 °C	0.62 ± 0.01	4.5 ± 0.2	0.3 ± 0.1	94 ± 8	65 ± 5
UCA–TiO ₂ 450 °C	0.57 ± 0.04	4.6 ± 0.4	0.3 ± 0.1	101 ± 3	70 ± 5
UCA–TiO ₂ 650 °C	0.57 ± 0.03	3.3 ± 0.8	0.3 ± 0.1	78 ± 3	55 ± 2
UCA–TiO ₂ Au 250 °C	0.49 ± 0.02	4.9 ± 0.1	0.2 ± 0.1	100 ± 5	68 ± 1
UCA–TiO ₂ Au 450 °C	0.48 ± 0.08	4.7 ± 0.3	0.5 ± 0.1	83 ± 5	54 ± 2
UCA–TiO ₂ Au 650 °C	0.51 ± 0.06	5.0 ± 0.1	0.2 ± 0.1	85 ± 7	55 ± 5

Since the reduced photocatalytic performances in the time (long-term use) is a considerable drawback of commercial material applied on stone, due to the loss of TiO₂ from the surface, we have also evaluated the degree of adhesion of the sols applied on limestone by peeling test. In Table 2 we reported the weight lost by the untreated stone and its treated counterparts. In particular, the untreated stone shows the greatest loss of mass after the adhesion testing (Table 2), due to a high amount of loose matter onto its surface, easily detached using the magic tape. All treated surfaces show almost negligible loss of mass (Table 2), confirming that the coatings are adhered firmly on the stone. Therefore, the inclusion of the photocatalyst in a mesoporous silica coating is an attractive solution to provide the long-term wear resistance, increasing the degree of particles adhesion to the surface. In addition, the considerable reduction of stone mass detached from surface indicates that the treatments also produce an effective consolidation of substrate surface.

We also investigated the mechanical resistance of stone by Vicker test. In particular, it was evaluated the enhanced strengthening of the stone due to the products applied. The histogram reported in Figure 5 shows the mechanical resistance of all stone samples under study. Some significant differences were observed. The treatments increase the stone hardness, confirming the substrate consolidation. The samples treated containing TiO₂ show resistance values higher to those obtained for the stone treated with only silica, probably due to the fact that TiO₂ is harder than silica. Comparing the materials with TiO₂/AuNRs, we observe that the UCA–TiO₂Au 450 °C sample produced the highest increase in stone resistance, about two times the value obtained for the untreated stone. These hardness variations observed for the treatments containing TiO₂ are attributable to the stone heterogeneities.

In particular, the penetration of water on the treated stone surface allows us to evaluate the hydrophobic properties of stone. Since the deterioration process of stone is mainly effected by water, the best surface protection is obtained when the coating on the exterior surface of the stone hinders the absorption of water [7]. Therefore, we have also measured water droplet static contact angles on the surface of treated limestone samples. The experimental results are given in Table 2. The untreated limestone sample shows water absorption due to the hydrophilic properties of the stone and its porosity. We observed that the treatments prevent the water absorption producing contact angles close to 90°. Again, the variations in values are attributable to the stone variability. The nearly hydrophobic behavior of the samples can be explained as the presence of non-hydrolyzed ethoxy groups in the coatings.

In order to evaluate the ability of the nanocomposites to prevent penetration of water into the limestone, the capillary water absorption test was carried out [38]. This experimental study was determined by plotting the absorbed water amount per cm² (Qi) vs. time for treated and untreated samples. The capillary absorption coefficient (WAC), the relative capillary index (RCI) and the Total

water uptake (TWU) values obtained after 48 h are shown in Table 3. The obtained results confirm that coatings effectively prevent the penetration of water into the stone pores, due to a pore-filling effect produced by the coating, since the uptake values, CA and RCI obtained for all the treated samples is significantly lower than the value those obtained for the untreated counterpart. Specifically, water capillarity absorption coefficient (WAC 0–60 min) decreased by about 90% for UCA–TiO₂ and UCA–TiO₂Au series. The Relative Capillary Index (RCI) after 6 days decreased by 70%–80% for all samples under study compared to untreated stone. The differences in capillary absorption between the several materials are small, in agreement with the natural stone heterogeneity.

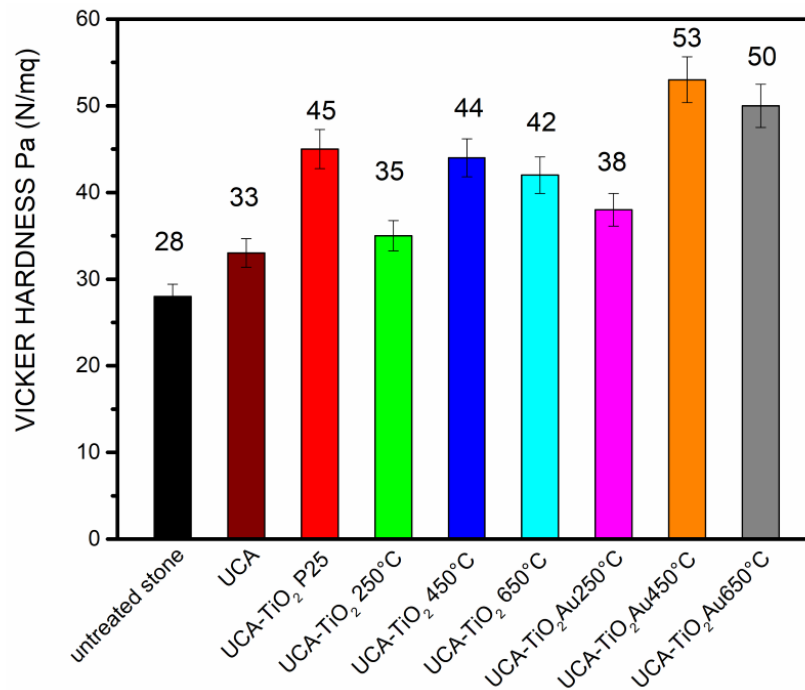


Figure 5. Histogram of mechanical resistance obtained by Vicker test, for the limestone under study after the application of our photocatalyst.

Table 3. Determination of water absorption coefficient (WAC), relative capillary index (RCI) and total water uptake values (TWU) obtained after 48 h by capillarity, according to UNI-EN 15801:2010 [38].

Sample	WAC 0–60 min ± 0.01	RCI 0–144 h ± 0.05	TWU (% w/w)
Untreated stone	2.83	1	3.50 ± 0.55
UCA	0.65	0.85	1.03 ± 0.40
UCA–TiO ₂ P25	0.11	0.21	0.17 ± 0.08
UCA–TiO ₂ 250 °C	0.10	0.10	0.11 ± 0.03
UCA–TiO ₂ 450 °C	0.23	0.70	0.74 ± 0.02
UCA–TiO ₂ 650 °C	0.20	0.40	0.55 ± 0.01
UCA–TiO ₂ Au 250 °C	0.14	0.30	0.36 ± 0.03
UCA–TiO ₂ Au 450 °C	0.24	0.34	0.52 ± 0.01
UCA–TiO ₂ Au 650 °C	0.11	0.12	0.16 ± 0.05

We wish to remark that the samples employed in the photocatalytic tests lost their hydrophobic behavior, with their angles becoming lower than 90° (Table 2). The high temperature and humidity inside degradation chamber promoted the hydrolysis of remaining ethoxy groups. However, the samples preserved their properties against the water penetration; despite the fact that the surface is not hydrophobic, the coating filling the pores blocked the passage of water.

3.4. Photocatalysis Experiments

The self-cleaning properties of the synthesized photocatalysts were investigated by measuring the photodegradation of a target staining molecule, Methylene blue (MB), under simulated solar light, deposited previously on the stone surface. MB was dissolved in ethanol ensuring a rapid evaporation of all the liquid. The photodegradation evolution of MB was recorded with the time, and the results are shown in Figure 6a, for each photocatalyst under study. Limestone samples treated with UCA and UCA-TiO₂ P25 coatings and untreated samples were used as comparison and reference counterparts, respectively. The photocatalytic activity is expressed as Relative Absorbance, which is given by the following expression: A/A_0 , where A_0 is the value obtained for the maximum absorbance of the samples at the beginning of the test ($t = 0$ h), while A corresponds to the same measurements recorded at each irradiation time. This test was carried out at 60 °C, in presence of atmospheric oxygen, without liquid water and with around 50% relative humidity (RH) values, the humidity is fundamental for the generation of OH free radicals. The obtained results are plotted in Figure 6a.

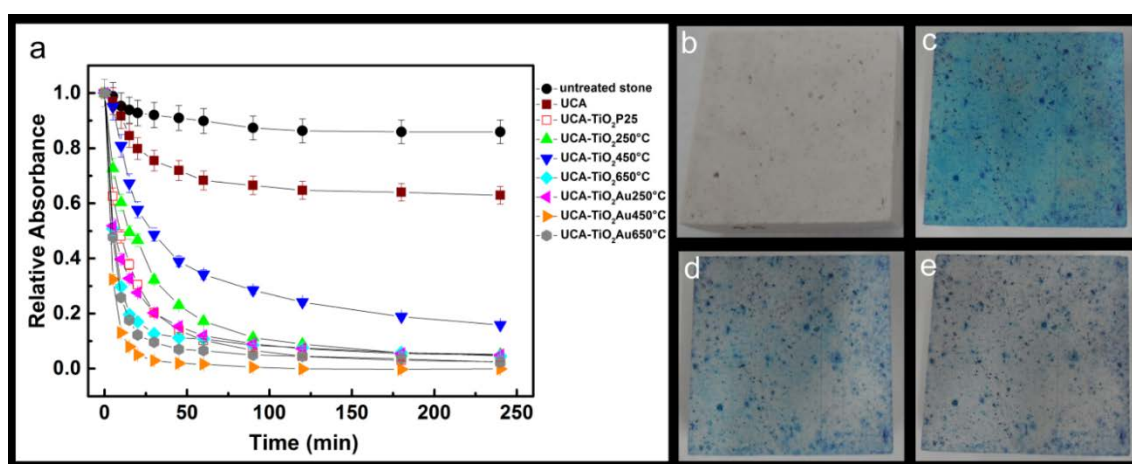


Figure 6. (a) Evolution of photocatalytic degradation of Methylene blue (MB) on stone specimens treated with UCA-TiO₂ and UCA-TiO₂Au series, UCA-TiO₂ P25 as reference material, as well as the untreated specimen. Each data point is the mean of three replicates. MB degradation on the stone treated with UCA-TiO₂Au 450 °C obtained at different irradiation times: untreated stone (b), 0 min (c), 30 min (d) and 60 min (e).

Photocatalytic degradation runs were preceded by blank test on untreated samples or in the absence of a photocatalyst (UCA). Both samples showed a slight MB degradation due to a photochemical mechanism [62]. The faster degradation in the UCA-treated samples is due to two reasons: the coating prevents the MB penetration inside the substrate and it promotes the MB adsorption in monomer form, which makes the degradation rate faster than the dimer in untreated stone [28]. All samples containing TiO₂ improved the MB degradation, demonstrating the TiO₂ photoactivity and confirming the effectiveness of these novel nanomaterials as self-cleaning agents. In detail, all samples produced a nearly 100% MB degradation after 240 min of irradiation; however the main difference between the samples was the degradation rate, which was especially observed in the first stage of reaction. UCA-TiO₂Au 450 °C reached nearly 90% of degradation in 10 min whereas UCA-TiO₂ 250 °C and UCA-TiO₂ 650 °C reached 40 and 70% respectively in the same time interval. In addition, to better highlight the different catalytic activity of the coatings, the kinetic constants of MB decoloration for all investigated samples is reported in Table 4. In particular, the rate of the reaction assisted by UCA-TiO₂Au 450 °C is 3.7 times higher than that catalyzed by UCA-TiO₂ 250 °C, 1.6 times higher than UCA-TiO₂ 650 °C and 2.6 times higher than UCA-TiO₂ P25. Therefore, the extent of MB photocatalytic degradation assisted by this series of nanomaterials could be summarized as follows:

UCA-TiO₂Au 450 °C > UCA-TiO₂Au 650 °C > UCA-TiO₂ 650 °C > UCA-TiO₂ P25 = UCA-TiO₂Au 250 °C > UCA-TiO₂ 250 °C > UCA-TiO₂ 450 °C.

Table 4. Kinetic constants for the MB decoloration process of UCA-TiO₂Au samples nanocomposites in comparison with UCA-TiO₂ calcinated at 250 °C, 450 °C and 650 °C, respectively and UCA-TiO₂ P25.

Samples	$K_{\text{kinetic}} \text{ (min}^{-1}\text{)}$
untreated stone	$0.004 \pm 1 \cdot 10^{-3}$
UCA	$0.010 \pm 1 \cdot 10^{-3}$
UCA-TiO ₂ P25	$0.069 \pm 4 \cdot 10^{-3}$
UCA-TiO ₂ 250 °C	$0.049 \pm 2 \cdot 10^{-3}$
UCA-TiO ₂ 450 °C	$0.024 \pm 2 \cdot 10^{-3}$
UCA-TiO ₂ 650 °C	$0.114 \pm 4 \cdot 10^{-3}$
UCA-TiO ₂ Au 250 °C	$0.084 \pm 8 \cdot 10^{-3}$
UCA-TiO ₂ Au 450 °C	$0.183 \pm 8 \cdot 10^{-3}$
UCA-TiO ₂ Au 650 °C	$0.124 \pm 6 \cdot 10^{-3}$

The coatings containing TiO₂/Au were more effective than the corresponding ones with TiO₂ confirming the enhancement of TiO₂ photoactivity produced by gold, as previously reported [28]. By comparing the products with TiO₂/AuNRs, faster degradation was observed for stone treated with UCA-TiO₂Au 450 °C. Figure 6b–e shows the evolution of the stained surface for this sample. Its higher activity can be attributed to the presence of AuNRs with anisotropic shape whereas UCA-TiO₂Au 650 °C contains spherical NPs with lower absorbance in the visible range. Additionally, the calcination at high temperature promotes the rutile formation and the growing of particles reducing the TiO₂ photoactivity [63]. It is remarkable that UCA-TiO₂ 450 °C showed a MB degradation considerably lower than the other TiO₂ samples. This behavior can be related to the anomalous characterization results previously reported for these xerogels. Probably, its unfavorable textural parameters were particularly responsible; its surface area that was nearly a third of the value for the other samples.

Furthermore, each coating was applied on three samples that were stained with carbon soot. The photocatalytic degradation performance was tested by studying the photodegradation of soot under simulated solar light irradiation. Specifically, the soot can be oxidized following two pathways: a direct single step and a serial sequence through a solid intermediate species, which is subsequently oxidized to CO₂. The evaluation of the photocatalytic performance was evaluated by means of absorbance measurements and reported in terms of relative absorbance A/A_0 vs. time. Experimental data point out that UCA-TiO₂Au 450 °C is the best performing coating for soot degradation with the percentage of 25% compared to untreated stone with almost 0%. In this case, it was not possible to calculate the kinetics constants due to the lack of points in the first stage of reaction; however, considering the first 30 min of reaction, it can be observed that UCA-TiO₂Au 450 °C catalyzed an 18% degradation of soot, i.e., 1.4 and 1.5 times higher than UCA-TiO₂Au 650 °C and UCA-TiO₂ 650 °C, respectively.

Figure 7b,c shows the color differences under solar simulated light at two different irradiation times, 0 min (b) and 340 h min (c), for the UCA-TiO₂Au 450 °C coating. In the case of limestone samples treated with the UCA-TiO₂ and UCA-TiO₂Au series at 450 °C and 650 °C, we observed that gold produced an increase in the amount of soot removed after 340 h under simulated solar irradiation (Figure 7a). In particular, UCA-TiO₂Au 450 °C removed an amount of soot 50% higher than UCA-TiO₂ 450 °C, while the increase for UCA-TiO₂Au 650 °C respect to UCA-TiO₂ 650 °C was a 30%. This confirmed, again, the enhancement in TiO₂ photoactivity produced by gold. On the other hand, the soot degradation profiles obtained for UCA-TiO₂ 250 °C and UCA-TiO₂Au250 °C samples show a trend similar to that of the untreated stone. This may be due to the low calcination temperature producing TiO₂ not completely crystalline with low activity. The extent of soot photocatalytic degradation assisted by UCA-TiO₂ and UCA-TiO₂AuNRs nanomaterials could be summarized

as follow: UCA–TiO₂Au 450 °C > UCA–TiO₂Au 650 °C > UCA–TiO₂ 650 °C = UCA–TiO₂ 450 °C > UCA–TiO₂ P25 > UCA > UCA–TiO₂ 250 °C = UCA–TiO₂Au 250 °C = Untreated stone.

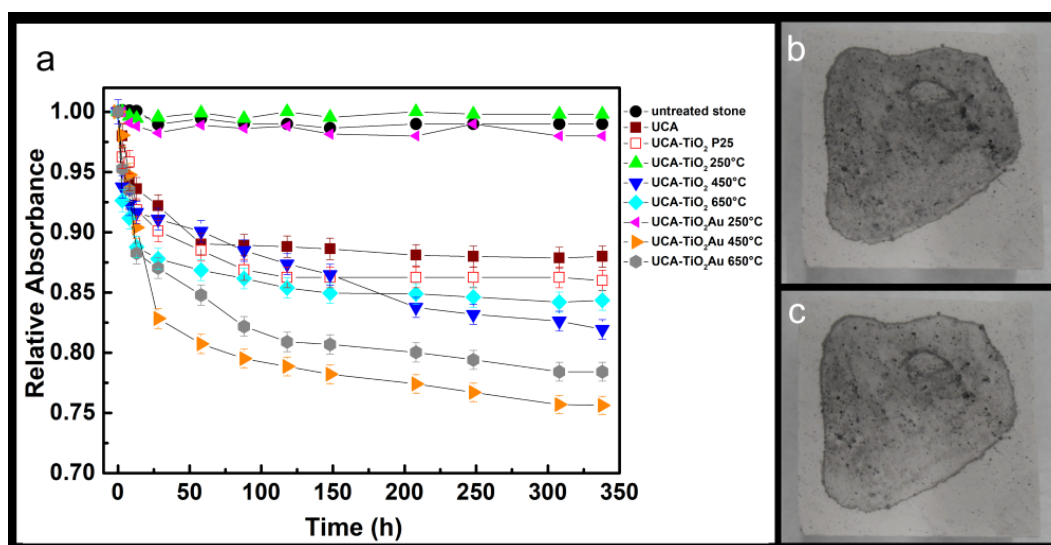


Figure 7. (a) Photocatalytic soot oxidation of each material under study reported in terms of relative absorbance A/A_0 vs. time. Each data point is the mean of three replicates. Soot degradation on the stone treated with UCA–TiO₂Au 450 °C obtained at different irradiation times: (b) 0 min and (c) 340 h.

4. Conclusions

We have synthesized and characterized an innovative photoactive and hydrophobic TiO₂/AuNRs–SiO₂ nanocomposite for self-cleaning application. Briefly, we used a simple and practical synthetic method, which consists of mixing silicon alkoxides and preformed TiO₂/AuNRs in the presence of *n*-octylamine. The SiO₂ matrix acts as an absorber and provides access to the TiO₂/AuNRs photocatalytic sites, and it does not affect the AuNR size/shape and does not modify the LSPR of AuNRs in the preformed materials. Interestingly, all the formulations improved the mechanical strength of the stone without altering their aesthetical and chemical-physical properties to a significant extent. Furthermore, the photoactivity of TiO₂/AuNRs–SiO₂ nanocomposites was affected by the morphology of TiO₂/AuNRs, which changed by varying calcination temperature. At 250 °C and 450 °C Au NRs preserved their anisotropy, while at 650 °C they are transformed from nanorods to spheres and ellipsoids during preparation procedure of TiO₂/AuNRs nanomaterial. The most suitable calcination temperature to achieve catalysts with a high photoactivity is 450 °C, probably due to an improved contact between the metal and semiconductor nanoparticles established during temperature annealing. Indeed, from our investigation, we conclude that the anisotropy of Au in TiO₂ is an essential factor for improving the photoactivity of the TiO₂/AuNRs–SiO₂ nanocomposites.

In particular, UCA–TiO₂Au 450 °C was the best performing coating with self-cleaning properties and also the ability to remove soot. Therefore, we believe that these materials can be exploited in applications as protective products for building materials, due to their self-cleaning and hydrophobic properties, which meet user requirements to preserve the aesthetic properties of stone.

Supplementary Materials: The following are available online at <http://www.mdpi.com/2079-6412/8/9/296/s1>, Figure S1: (A) UV-Vis absorption spectra of Au NRs solution, after purification in order to remove excess of CTAB; (B) Transmission electron microscopy image of the Au NRs, Figure S2: TEM micrograph of TiO₂/AuNRs photocatalysts for different synthesis conditions: TiO₂/AuNRs 250 °C (A); TiO₂/AuNRs 450 °C (B); TiO₂/AuNRs 650 °C (C), Figure S3: Diffuse reflectance spectra (DRS) of TiO₂/Au NRs nanocomposites deposited onto quartz slides, recorded in absorption mode, Figure S4: XPD patterns of the UCA–TiO₂ and UCA–TiO₂Au nanocomposites under study. (a,c) Original data of compounds; (b,d) Data corrected by subtracting the contribution of UCA component to enhance the contribution of the TiO₂ nanocrystals and Au NRs, Figure S5. Representative pictures

of the stones before and after coating: (A) untreated; (B) UCA–TiO₂ P25; (C) UCA–TiO₂ 450 °C; (D) UCA–TiO₂/Au NRs 450 °C.

Author Contributions: A.T., M.L., R.C. and M.J.M. conceived and designed the experiments. A.T., M.L., F.P., A.F., C.G. performed the experiments. A.T., M.L., F.P., C.G., R.C. and M.J.M. analyzed the data. R.C. and M.J.M. contributed reagents/materials/analysis tools; A.T., R.C., M.L., C.G. and M.J.M. wrote the paper.

Funding: This work was funded by the Apulia Region FOTOCATALIZZATORI NANOSTRUTTURATI E RADIAZIONE UV PER UN'ACQUA PIÙ PULITA" (WOBV6K5), the Project "FONTANAPULIA—INNOVACONCRETE—Innovative Materials and Techniques for the Conservation of 20th Century Concrete-based Cultural Heritage" H2020-NMPB-35-2017 (760858-2) and the Spanish Government/FEDER-EU (MAT2013-42934-R and MAT2017-84228-R). M.L. would also like to thank MINECO for his pre-doctoral grant (BES-2014-068031).

Acknowledgments: Francesco Baldassarre is acknowledged for technical assistance for X-ray Powder Diffraction (XPD).

Conflicts of Interest: The authors declare no conflicts of interest. The founding sponsors had no role in the design of the study; in the collection, analyses, or interpretation of data; in the writing of the manuscript, and in the decision to publish the results.

References

1. Pinho, L.; Mosquera, M.J. Photocatalytic activity of TiO₂-SiO₂ nanocomposites applied to buildings: Influence of particle size and loading. *Appl. Catal. B Environ.* **2013**, *134–135*, 205–221. [[CrossRef](#)]
2. Munafò, P.; Goffredo, G.B.; Quagliarini, E. TiO₂-based nanocoatings for preserving architectural stone surfaces: An overview. *Constr. Build. Mater.* **2015**, *84*, 201–218. [[CrossRef](#)]
3. International Council on Monuments and Sites-International Scientific Committee for Stone (ICOMOS-ISCS). *Illustrated Glossary on Stone Deterioration Patterns*; ICOMOS: Charenton-le-Pont, France, 2010.
4. Petronella, F.; Truppi, A.; Ingrosso, C.; Placido, T.; Striccoli, M.; Curri, M.L.; Agostiano, A.; Comparelli, R. Nanocomposite materials for photocatalytic degradation of pollutants. *Catal. Today* **2017**, *281*, 85–100. [[CrossRef](#)]
5. Truppi, A.; Petronella, F.; Placido, T.; Striccoli, M.; Agostiano, A.; Curri, M.; Comparelli, R. Visible-Light-Active TiO₂-Based Hybrid Nanocatalysts for Environmental Applications. *Catalysts* **2017**, *7*, 100. [[CrossRef](#)]
6. Chen, J.; Poon, C.S. Photocatalytic construction and building materials: From fundamentals to applications. *Build. Environ.* **2009**, *44*, 1899–1906. [[CrossRef](#)]
7. Colangiuli, D.; Calia, A.; Bianco, N. Novel multifunctional coatings with photocatalytic and hydrophobic properties for the preservation of the stone building heritage. *Constr. Build. Mater.* **2015**, *93*, 189–196. [[CrossRef](#)]
8. Midtdal, K.; Jelle, B.P. Self-cleaning glazing products: A state-of-the-art review and future research pathways. *Sol. Energy Mater. Sol. Cells* **2013**, *109*, 126–141. [[CrossRef](#)]
9. Smits, M.; Tytgat, T.; Craeye, B.; Costarramone, N.; Lacombe, S.; Lenaerts, S. Photocatalytic degradation of soot deposition: Self-cleaning effect on titanium dioxide coated cementitious materials. *Chem. Eng. J.* **2013**, *222*, 411–418. [[CrossRef](#)]
10. Mills, A.; Wang, J.; Crow, M. Photocatalytic oxidation of soot by P25 TiO₂ films. *Chemosphere* **2006**, *64*, 1032–1035. [[CrossRef](#)] [[PubMed](#)]
11. Chin, P.; Roberts, G.W.; Ollis, D.F. Kinetic Modeling of Photocatalyzed Soot Oxidation on Titanium Dioxide Thin Films. *Ind. Eng. Chem. Res.* **2007**, *46*, 7598–7604. [[CrossRef](#)]
12. Chin, P.; Grant, C.S.; Ollis, D.F. Quantitative photocatalyzed soot oxidation on titanium dioxide. *Appl. Catal. B Environ.* **2009**, *87*, 220–229. [[CrossRef](#)]
13. Herrmann, J.M. Photocatalysis fundamentals revisited to avoid several misconceptions. *Appl. Catal. B Environ.* **2010**, *99*, 461–468. [[CrossRef](#)]
14. Kochuveedu, S.T.; Jang, Y.H.; Kim, D.H. A study on the mechanism for the interaction of light with noble metal-metal oxide semiconductor nanostructures for various photophysical applications. *Chem. Soc. Rev.* **2013**, *42*. [[CrossRef](#)] [[PubMed](#)]
15. Fujishima, A.; Zhang, X.; Tryk, D.A. TiO₂ photocatalysis and related surface phenomena. *Surf. Sci. Rep.* **2008**, *63*, 515–582. [[CrossRef](#)]

16. Ochiai, T.; Fujishima, A. Photoelectrochemical properties of TiO₂ photocatalyst and its applications for environmental purification. *J. Photochem. Photobiol. C* **2012**, *13*, 247–262. [[CrossRef](#)]
17. Petronella, F.; Curri, M.L.; Striccoli, M.; Fanizza, E.; Mateo-Mateo, C.; Alvarez-Puebla, R.A.; Sibillano, T.; Giannini, C.; Correa-Duarte, M.A.; Comparelli, R. Direct growth of shape controlled TiO₂ nanocrystals onto SWCNTs for highly active photocatalytic materials in the visible. *Appl. Catal. B Environ.* **2015**, *178*, 91–99. [[CrossRef](#)]
18. Binas, V.; Venieri, D.; Kotzias, D.; Kiriakidis, G. Modified TiO₂ based photocatalysts for improved air and health quality. *J. Mater.* **2017**, *3*, 3–16. [[CrossRef](#)]
19. Byrne, C.; Subramanian, G.; Pillai, S.C. Recent advances in photocatalysis for environmental applications. *J. Environ. Chem. Eng.* **2018**, *6*, 3531–3555. [[CrossRef](#)]
20. Wang, H.; Zhang, L.; Chen, Z.; Hu, J.; Li, S.; Wang, Z.; Liu, J.; Wang, X. Semiconductor heterojunction photocatalysts: Design, construction, and photocatalytic performances. *Chem. Soc. Rev.* **2014**, *43*. [[CrossRef](#)] [[PubMed](#)]
21. Zhang, X.; Chen, Y.L.; Liu, R.-S.; Tsai, D.P. Plasmonic photocatalysis. *Rep. Prog. Phys.* **2013**, *76*. [[CrossRef](#)] [[PubMed](#)]
22. Pelaez, M.; Nolan, N.T.; Pillai, S.C.; Seery, M.K.; Falaras, P.; Kontos, A.G.; Dunlop, P.S.M.; Hamilton, J.W.J.; Byrne, J.A.; O'Shea, K.; et al. A review on the visible light active titanium dioxide photocatalysts for environmental applications. *Appl. Catal. B Environ.* **2012**, *125*, 331–349. [[CrossRef](#)]
23. Eustis, S.; El-Sayed, M.A. Why gold nanoparticles are more precious than pretty gold: Noble metal surface plasmon resonance and its enhancement of the radiative and nonradiative properties of nanocrystals of different shapes. *Chem. Soc. Rev.* **2006**, *35*, 209–217. [[CrossRef](#)] [[PubMed](#)]
24. Bumajdad, A.; Madkour, M. Understanding the superior photocatalytic activity of noble metals modified titania under UV and visible light irradiation. *Phys. Chem. Chem. Phys.* **2014**, *16*. [[CrossRef](#)] [[PubMed](#)]
25. Zhang, X.; Zhu, Y.; Yang, X.; Wang, S.; Shen, J.; Lin, B.; Li, C. Enhanced visible light photocatalytic activity of interlayer-isolated triplex Ag@SiO₂@TiO₂ core-shell nanoparticles. *Nanoscale* **2013**, *5*. [[CrossRef](#)] [[PubMed](#)]
26. Kapridaki, C.; Pinho, L.; Mosquera, M.J.; Maravelaki-Kalaitzaki, P. Producing photoactive, transparent and hydrophobic SiO₂-crystalline TiO₂ nanocomposites at ambient conditions with application as self-cleaning coatings. *Appl. Catal. B Environ.* **2014**, *156–157*, 416–427. [[CrossRef](#)]
27. Pakdel, E.; Daoud, W.A.; Afrin, T.; Sun, L.; Wang, X. Self-cleaning wool: Effect of noble metals and silica on visible-light-induced functionalities of nano TiO₂ colloid. *J. Text. Inst.* **2015**, *106*, 1348–1361. [[CrossRef](#)]
28. Luna, M.; Delgado, J.; Gil, M.L.A.; Mosquera, M. TiO₂-SiO₂ Coatings with a Low Content of AuNPs for Producing Self-Cleaning Building Materials. *Nanomaterials* **2018**, *8*, 177. [[CrossRef](#)] [[PubMed](#)]
29. Pinho, L.; Mosquera, M.J. Titania-Silica Nanocomposite Photocatalysts with Application in Stone Self-Cleaning. *J. Phys. Chem. C* **2011**, *115*, 22851–22862. [[CrossRef](#)]
30. Facio, D.S.; Luna, M.; Mosquera, M.J. Facile preparation of mesoporous silica monoliths by an inverse micelle mechanism. *Microporous Mesoporous Mater.* **2017**, *247*, 166–176. [[CrossRef](#)]
31. Ancora, R.; Borsa, M.; Cassar, L. WO/2009/080647 Titanium Dioxide Based Photocatalytic Composites and Derived Products on a Metakaolin Support; Italcementi: Bergamo, Italy, 2009.
32. De Sio, L.; Caracciolo, G.; Annesi, F.; Placido, T.; Pozzi, D.; Comparelli, R.; Pane, A.; Curri, M.L.; Agostiano, A.; Bartolino, R. Photo-thermal effects in gold nanorods/DNA complexes. *Micro Nano Syst. Lett.* **2015**, *3*. [[CrossRef](#)]
33. Thommes, M.; Smarsly, B.; Groenewolt, M.; Ravikovitch, P.I.; Neimark, A.V. Adsorption Hysteresis of Nitrogen and Argon in Pore Networks and Characterization of Novel Micro and Mesoporous Silicas. *Langmuir* **2006**, *22*, 756–764. [[CrossRef](#)] [[PubMed](#)]
34. Tauc, J. Optical properties and electronic structure of amorphous Ge and Si. *Mater. Res. Bull.* **1968**, *3*, 37–46. [[CrossRef](#)]
35. Tandon, S.P.; Gupta, J.P. Measurement of Forbidden Energy Gap of Semiconductors by Diffuse Reflectance Spectra. *Phys. Status Solidi B* **1970**, *38*, 363–367. [[CrossRef](#)]
36. Drdácák, M.; Lesák, J.; Rescic, S.; Slížková, Z.; Tiano, P.; Valach, J. Standardization of peeling tests for assessing the cohesion and consolidation characteristics of historic stone surfaces. *Mater. Struct.* **2012**, *45*, 505–520. [[CrossRef](#)] [[PubMed](#)]
37. ASTM C1327-15-Standard Test Method for Vickers Indentation Hardness of Advanced Ceramics; ASTM: West Conshohocken, PA, USA, 2015.

38. UNI-EN 15801: *Conservation of Cultural Property—Test Methods—Determination of Water Absorption by Capillarity*; Italian Standards: Milan, Italy, 2010.
39. UNI-EN 15886: *Conservation of Cultural Property—Test Methods—Colour Measurement of Surfaces*; Italian Standards: Milan, Italy, 2010.
40. Berns, R.S. *Billmeyer and Saltzman's Principles of Color Technology*; Wiley-Interscience: New York, NY, USA, 2000.
41. Smits, M.; Huygh, D.; Craeye, B.; Lenaerts, S. Effect of process parameters on the photocatalytic soot degradation on self-cleaning cementitious materials. *Catal. Today* **2014**, *230*, 250–255. [[CrossRef](#)]
42. Vasiliev, P.O.; Faure, B.; Ng, J.B.S.; Bergström, L. Colloidal aspects relating to direct incorporation of TiO₂ nanoparticles into mesoporous spheres by an aerosol-assisted process. *J. Colloid Interface Sci.* **2008**, *319*, 144–151. [[CrossRef](#)] [[PubMed](#)]
43. Pinho, L.; Elhaddad, F.; Facio, D.S.; Mosquera, M.J. A novel TiO₂-SiO₂ nanocomposite converts a very friable stone into a self-cleaning building material. *Appl. Surf. Sci.* **2013**, *275*, 389–396. [[CrossRef](#)]
44. Sekhar, Y.R.; Sharma, K.V. Study of viscosity and specific heat capacity characteristics of water-based Al₂O₃ nanofluids at low particle concentrations. *J. Exp. Nanosci.* **2015**, *10*, 86–102. [[CrossRef](#)]
45. Giannini, C.; Ladisa, M.; Altamura, D.; Siliqi, D.; Sibillano, T.; De Caro, L. X-ray Diffraction: A Powerful Technique for the Multiple-Length-Scale Structural Analysis of Nanomaterials. *Crystals* **2016**, *6*, 87. [[CrossRef](#)]
46. Amendola, V.; Pilot, R.; Frascioni, M.; Maragò, O.M.; Iati, M.A. Surface plasmon resonance in gold nanoparticles: A review. *J. Phys. Condens. Matter* **2017**, *29*. [[CrossRef](#)] [[PubMed](#)]
47. Zou, R.; Zhang, Q.; Zhao, Q.; Peng, F.; Wang, H.; Yu, H.; Yang, J. Thermal stability of gold nanorods in an aqueous solution. *Colloids Surf. A* **2010**, *372*, 177–181. [[CrossRef](#)]
48. Liu, L.; Ouyang, S.; Ye, J. Gold-Nanorod-Photosensitized Titanium Dioxide with Wide-Range Visible-Light Harvesting Based on Localized Surface Plasmon Resonance. *Angew. Chem. Int. Ed.* **2013**, *52*, 6689–6693. [[CrossRef](#)] [[PubMed](#)]
49. Thommes, M.; Kaneko, K.; Neimark, A.V.; Olivier, J.P.; Rodriguez-Reinoso, F.; Rouquerol, J.; Sing, K.S.W. Physisorption of gases, with special reference to the evaluation of surface area and pore size distribution (IUPAC Technical Report). *Pure Appl. Chem.* **2015**, *87*, 1051–1069. [[CrossRef](#)]
50. Cychoz, K.A.; Guillet-Nicolas, R.; García-Martínez, J.; Thommes, M. Recent advances in the textural characterization of hierarchically structured nanoporous materials. *Chem. Soc. Rev.* **2017**. [[CrossRef](#)] [[PubMed](#)]
51. Pinho, L.; Rojas, M.; Mosquera, M.J. Ag-SiO₂-TiO₂ nanocomposite coatings with enhanced photoactivity for self-cleaning application on building materials. *Appl. Catal. B Environ.* **2015**, *178*, 144–154. [[CrossRef](#)]
52. Yamauchi, Y.; Takeuchi, F.; Todoroki, S.; Sakka, Y.; Inoue, S. Spherical Mesoporous Silica Particles with Titanium Dioxide Nanoparticles by an Aerosol-assisted Coassembly. *Chem. Lett.* **2008**, *37*, 72–73. [[CrossRef](#)]
53. Suzuki, N.; Jiang, X.; Radhakrishnan, L.; Takai, K.; Shimasaki, K.; Huang, Y.T.; Miyamoto, N.; Yamauchi, Y. Hybridization of Photoactive Titania Nanoparticles with Mesoporous Silica Nanoparticles and Investigation of Their Photocatalytic Activity. *Bull. Chem. Soc. Jpn.* **2011**, *84*, 812–817. [[CrossRef](#)]
54. Zhang, P.; Tian, J.; Xu, R.; Ma, G. Hydrophilicity, photocatalytic activity and stability of tetraethyl orthosilicate modified TiO₂ film on glazed ceramic surface. *Appl. Surf. Sci.* **2013**, *266*, 141–147. [[CrossRef](#)]
55. Ting, H.F.; Chen, C.M.; Lu, F.H.; Suen, S.Y. Adsorption and photodegradation of methylene blue using a bulk Ti material with porous titania layer prepared by chemical oxidation. *J. Taiwan Inst. Chem. Eng.* **2014**, *45*, 617–624. [[CrossRef](#)]
56. Jawad, A.H.; Mubarak, N.S.A.; Ishak, M.A.M.; Ismail, K.; Nawawi, W.I. Kinetics of photocatalytic decolorization of cationic dye using porous TiO₂ film. *J. Taibah Univ. Sci.* **2016**, *10*, 352–362. [[CrossRef](#)]
57. Zhang, J.; Grabstanowicz, L.R.; Gao, S.; Hosmane, N.S.; Huang, B.; Dai, Y.; Liu, D.; Xu, T. Visible-light photocatalytic SiO₂/TiO_{2-x} C_x/C nanoporous composites using TiCl₄ as the precursor for TiO₂ and polyhydroxyl tannin as the carbon source. *Catal. Sci. Technol.* **2012**, *2*, 390–399. [[CrossRef](#)]
58. Sopyan, I.; Watanabe, M.; Murasawa, S.; Hashimoto, K.; Fujishima, A. A film-type photocatalyst incorporating highly active TiO₂ powder and fluororesin binder: Photocatalytic activity and long-term stability. *J. Electroanal. Chem.* **1996**, *415*, 183–186. [[CrossRef](#)]
59. Fattakhova-Rohlfing, D.; Szeifert, J.M.; Yu, Q.; Kalousek, V.; Rathouský, J.; Bein, T. Low-Temperature Synthesis of Mesoporous Titania–Silica Films with Pre-Formed Anatase Nanocrystals. *Chem. Mater.* **2009**, *21*, 2410–2417. [[CrossRef](#)]

60. Beyers, E.; Biermans, E.; Ribbens, S.; De Witte, K.; Mertens, M.; Meynen, V.; Bals, S.; Van Tendeloo, G.; Vansant, E.F.; Cool, P. Combined TiO₂/SiO₂ mesoporous photocatalysts with location and phase controllable TiO₂ nanoparticles. *Appl. Catal. B Environ.* **2009**, *88*, 515–524. [[CrossRef](#)]
61. Miliani, C.; Velo-Simpson, M.L.; Scherer, G.W. Particle-modified consolidants: A study on the effect of particles on sol-gel properties and consolidation effectiveness. *J. Cult. Herit.* **2007**, *8*, 1–6. [[CrossRef](#)]
62. Mills, A.; Wang, J. Photobleaching of methylene blue sensitised by TiO₂: An ambiguous system? *J. Photochem. Photobiol. A Chem.* **1999**, *127*, 123–134. [[CrossRef](#)]
63. Wang, G.; Xu, L.; Zhang, J.; Yin, T.; Han, D. Enhanced photocatalytic activity of TiO₂ powders (P25) via calcination treatment. *Int. J. Photoenergy* **2012**, *2012*. [[CrossRef](#)]



© 2018 by the authors. Licensee MDPI, Basel, Switzerland. This article is an open access article distributed under the terms and conditions of the Creative Commons Attribution (CC BY) license (<http://creativecommons.org/licenses/by/4.0/>).